Characterisation of Carbon Nano spheres (CNSs) from Cooking Oil with Ferrocene Catalyst on Activated Carbon Surface

1*Asst.Lec. Aʾalaa, Baddai. Nashter , Ministry of Education, Iraq,

2*Asst.Lec. Montaha, Kadhim. Sultan , Ministry of Education, Iraq,

3*Asst.Lec. Hadeel, Jalal. Abbas , Ministry of Education, Iraq,

[1]alla.bdai1205a@ihcoedu.uobaghdad.edu.iq

[2]montaha.kazem1205a@ihcoedu.uobaghdad.edu.iq
[3]hadeel.jalal1205a@ihcoedu.uobaghdad.edu.iq

Send Article Date 19/5/2025 Date of acceptance of the article： 2025/ 18 / 5

Characterisation of Carbon Nano spheres (CNSs) from Cooking Oil with Ferrocene Catalyst on Activated Carbon Surface

1*Asst.Lec. A'alaa, Baddai. Nashter , Ministry of Education, Iraq,

2*Asst.Lec. Montaha, Kadhim. Sultan , Ministry of Education, Iraq,

3*Asst.Lec. Hadeel, Jalal. Abbas , Ministry of Education, Iraq,

[1]alla.bdai1205a@ihcoedu.uobaghdad.edu.iq

[2]montaha.kazem1205a@ihcoedu.uobaghdad.edu.iq

[3]hadeel.jalal1205a@ihcoedu.uobaghdad.edu.iq

Send Article Date 19/5/2025 Date of acceptance of the article : 2025/ 18 / 5

Abstract:

Carbon nanospheres (CNSs) are one of the groups of carbon nanotubes formed as a by-product in the manufacture of carbon nanotubes (CNTs). CNSs have a size between 50 nm to 1 μm and can be empty or filled balls. CNSs have dangling bonds that cause their reactive properties. CNSs are widely studied as catalyst supports, adsorbents, or battery and supercapacitor electrodes. This study synthesised CNSs using activated carbon (AC) support. The iron catalyst was derived from ferrocene, $Fe(C_5H_5)_2$. Meanwhile, cooking oil was used as a carbon source to form CNSs. The cooking oil, catalyst, and activated carbon mixture were then carbonised using an electrical furnace at 700°C for 1 hour with a nitrogen atmosphere. In this experiment, the initial catalyst concentration was varied from 2.5, 5, 7.5 and 10g catalyst/100 ml cooking oil, with the ratio

of activated carbon to cooking oil 1:3 (w/w)—product characterisation using XRD, BET surface area analysis, Raman spectroscopy, EDS, and XPS. The surface morphology of activated carbon was observed by SEM and TEM analysis, and the results showed that from the synthesis carried out, CNSs were formed, composed of C (002) and C (100). It can also be observed that the larger the catalyst used, the more CNSs were formed. As the amount of catalyst increased, the iron and oxygen content in the sample was also observed by EDS measurements; based on XPS analysis, there was no change in the composition of functional groups on the surface of AC. A decrease in the surface area of AC was observed in each sample, with a maximum reduction of 50%. This resulted in a decrease in the adsorption capacity when used as an adsorbent. Its performance was stable when the 2.5g/100mL sample was tested by cyclic voltammetry as a lithium battery anode.

key words: activated carbon, iron catalyst, cooking oil, CNSs

توصيف جزيئات الكربون النانوية CNSs (من زيت الطهي باستخدام محفز الفيروسين على سطح الكربون المنشط)

ملخص

تُعدّ جزيئات الكربون النانوية (CNSs) إحدى مجموعات أنابيب الكربون النانوية التي تُشكّل كمنتج ثانوي في تصنيع أنابيب الكربون النانوية (CNTs). يتراوح حجمها بين 50 nm الى 1 µm ، ويمكن أن تكون كرات فارغة أو مملوءة. تحتوي على روابط متدلية تُسبب خصائصها التفاعلية. تُدرس جزيئات الكربون النانوية على نطاق واسع كدعامات للمحفزات، أو مواد ماصة، أو أقطاب كهربائية للبطاريات والمكثفات الفائقة. وقد ركّبت هذه الدراسة جزيئات الكربون النانوية باستخدام دعامة الكربون المنشط (AC). استُخلص المحفز الحديدي من الفيروسين، Fe(C5H5)2. في هذه الأثناء، استُخدم زيت الطهي كمصدر للكربون لتكوين جزيئات الكربون النانوية. تم كربنة خليط زيت الطهي والمحفز والكربون المنشط باستخدام فرن كهربائي عند درجة حرارة 700 درجة مئوية لمدة ساعة واحدة في جو من النيتروجين. في هذه التجربة، تم تغيير تركيز المحفز الأولي من 2.5، 5، 7.5 و 10 جرام من المحفز / 100 مل من زيت الطهي، مع نسبة الكربون النشط إلى زيت الطهي 1:3 (وزن/وزن) - توصيف المنتج باستخدام XRD، وتحليل مساحة سطح BET، و مطيافية رامان، وEDS، وXPS. تم ملاحظة مورفولوجيا سطح الكربون المنشط من خلال تحليل المجهر الإلكتروني الماسح والمجهر الإلكتروني النافذ، وأظهرت النتائج أنه من خلال التركيب الذي تم إجراؤه، تم تكوين CNSs، مكونة من C (002) وC (100). ويمكن أيضًا ملاحظة أنه كلما زاد حجم المحفز المستخدم، زاد تكوين CNSs. مع زيادة كمية

المحفز، تم أيضًا ملاحظة محتوى الحديد والأكسجين في العينة من خلال قياسات EDS؛ بناءً على تحليل XPS، لم يكن هناك أي تغيير في تكوين المجموعات الوظيفية على سطح AC. لوحظ انخفاض في مساحة سطح AC في كل عينة، مع أقصى انخفاض بنسبة 50٪. أدى ذلك إلى انخفاض في سعة الامتصاص عند استخدامه كمادة ماصة. كان أداؤه مستقرًا عند اختبار العينة 2.5 جم / 100 مل بواسطة الفولتميتر الدوري كأنود بطارية ليثيوم.
الكلمات المفتاحية: الكربون المنشط، محفز الحديد، زيت الطهي، CNSs

Introduction :

Carbon nanosphere (CNSs) are by-products of the manufacture of CNTs. Carbon atoms' pentagonal and hexagonal arrangement, in addition to forming shapes such as CNTs and CNFs, can also form CNSs [1]. Based on their size, these spherical structures can be distinguished into Cn and graphitic carbon onions with diameters between 2-20nm, carbon nanospheres with a lower graphitic structure with a diameter between 50nm-1□m, and carbon beads with a diameter above 1□m [2]. The structure of CNSs is unique because the sphere shape is not perfectly closed, so there are many dangling bonds [3]. This provides high chemical activity so CNSs can be used for various applications, such as catalyst support, adsorbent in wastewater treatment, and electrochemical capacitors [4].

Several researchers [5-7] have synthesised CNSs using ferrocene as a catalyst. Hans Kristianto et al. (2015) [8] synthesised CNSs using ferrocene as a catalyst and carbon source. Hollow CNSs were successfully synthesised using ferrocene at a pyrolysis temperature of 700^{o}C for 1 hour in a nitrogen atmosphere autoclave. The synthesised CNSs had a 50-150nm diameter with a wall thickness of 15nm. Yi et al. (2005)[9] carried out synthesis with various hydrocarbon sources such as styrene, toluene, benzene, hexane, cyclohexane, and ethane. The synthesis was carried out by the CVD method at temperatures between 900 to 1200^{o}C. At a catalyst concentration of 0.5% by weight, the main product was CNSs, and several CNTs were observed, while at a concentration of 3.5%, the main product was CNTs. In addition to the catalyst concentration, the amount of feed fed into the reactor determines the product obtained. In the study of Zhang et al. (2010) [10], at a carbon source that was too little or too much, the product obtained was CNSs or CNTs with a relatively short length or amorphous carbon. The research conditions used were a quartz reactor with two heating zones. Acetylene feed

was fed continuously with argon gas; the reaction temperature was 1050^{o}C, with a ferrocene catalyst.

Hans Kristianto et al. (2015) research has been conducted on the variation of concentration and method of catalyst deposition on the surface of AC to synthesise CNSs. Fe $(NO_3)_3.9H_2O$ catalyst deposition by the impregnation method successfully synthesised CNSs along with the increase in the amount of catalyst, from 5, 7.5 and 10% w/w, the CNSs obtained are increasing. However, it is not homogeneous on the entire surface of AC. Another method by Náfrádi et al (2016) [12] that has been used is catalyst deposition using the urea coprecipitation method, with an iron: urea ratio of 1:3. In this study, the initial concentration of the catalyst was varied, namely 10, 20, and 30% w/w to activated carbon. From the results of the SEM analysis, it can be seen that increasing the catalyst increases the number of CNSs deposited on the surface of AC. From the XRD results (not shown here), it is known that C(100) is formed, which is seen at the 2θ peak (43˚). This indicates the formation of the C sp^2 configuration commonly found in CNSs (Han, Jung et al., 2014). Observation of the characteristics of CNSs can be done by several methods, namely SEM and TEM, to see the morphology and diameter, then XRD and Raman Spectroscopy to know the degree of graphitisation (Nieto-Marquez, Romero et al., 2010). According to Lou et al. (2020) [11], this is due to the structure of CNSs, which have reactive edges and tend to form a combination of several spheres. In previous studies, CNSs were synthesised on the surface of AC support with an iron catalyst from Fe $(NO_3)_3.9H_2O$ using the impregnation catalyst deposition method [13] and urea coprecipitation deposition [14]. CNSs are made using precursors derived from biomass, namely cooking oil. Several researchers have carried out the manufacture of nanocarbon from biomass raw materials [8, 14]. However, it is still rarer than simpler carbon raw materials, such as benzene, toluene, acetylene, etc. Meanwhile, manufacturing CNSs with activated carbon support is the first time it has been done. The CNSs synthesis method is a simple pyrolysis method, where the precursor is not fed continuously but in batches, namely at the beginning before pyrolysis.

Based on the above discussion, the current research is being developed to study the characteristics of CNSs obtained from cooking oil precursors with ferrocene iron catalysts on the surface of AC and the effect of the initial concentration of iron catalysts on the CNS products obtained.

2. Materials and methods

2.1. Research design.

The materials used are Activated carbon (Merck), Ferrocene [$Fe(C_5H_5)_2(s)$], Aquades & N_2 gas. They were cooking Oil. The research aims to determine the operating conditions for manufacturing CNSs with activated carbon support. The support used is commercial activated carbon (Merck, India), using ferrocene catalyst $Fe(C_5H_5)_2$ (Sigma Aldrich), and commercial cooking oil (Rice Bran oil, Henan co. Iraq) as a carbon source.

In general, the steps of this research are divided into two parts: catalyst deposition and CNS synthesis. CNSs synthesis is carried out by mixing cooking oil, activated carbon and ferrocene, then pyrolysed at a temperature of 700°C for 1 hour in a nitrogen atmosphere, with a nitrogen flow rate of 1L/min. The sample is then allowed to cool in a nitrogen atmosphere before removal. The dried product is stored in a desiccator. The experiment was conducted by varying the catalyst ratio, namely 2.5, 5, 7.5 and 10g catalyst/100 ml cooking oil, with the ratio of activated carbon to cooking oil, 1:3 (w/w). The products obtained were characterised using XRD (Bruker D8 Advance, Cu-Kα radiation), SEM-EDS (JEOL JSM-7800F is equipped with EDS), XPS (PHI 5000 VersaProbe III, with an Al-Kα X-ray source at 117.4eV) TEM (JEOL JEM2100), Raman tests (Wasatch Photonics 405nm Raman Spectrometer) and Surface area test using the BET method (Micromeritics apparatus NOVA 1000/3200e Quanta chrome). Synthesis of CNSs with ferrocene iron catalyst shown in the following scheme-1

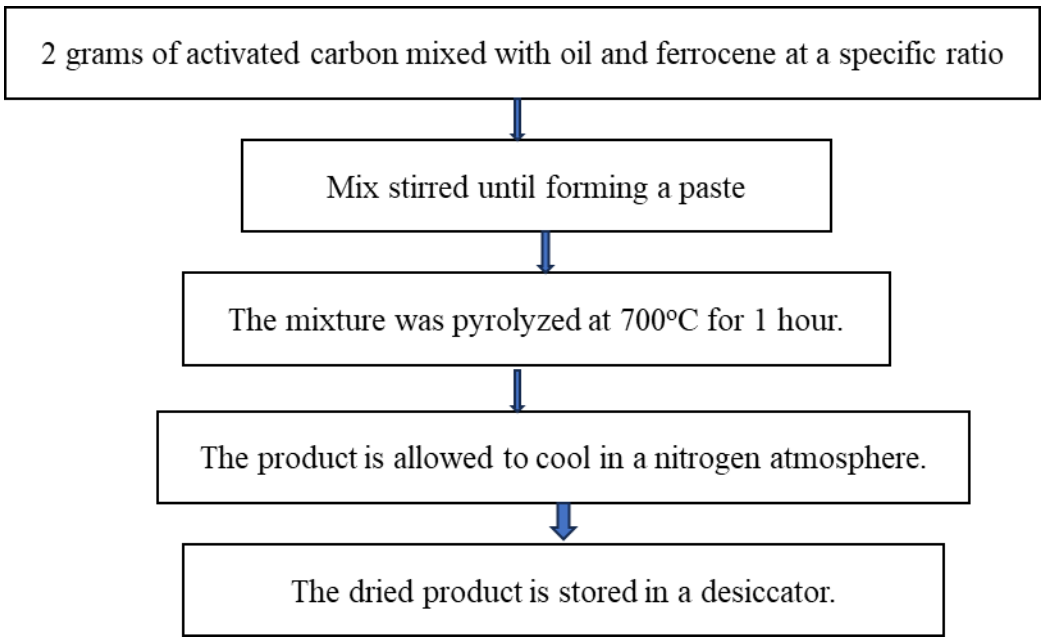

Scheme-1. How the iron catalyst deposition works on the surface of AC

The adsorption performance test with methylene blue is shown in the following scheme: 2

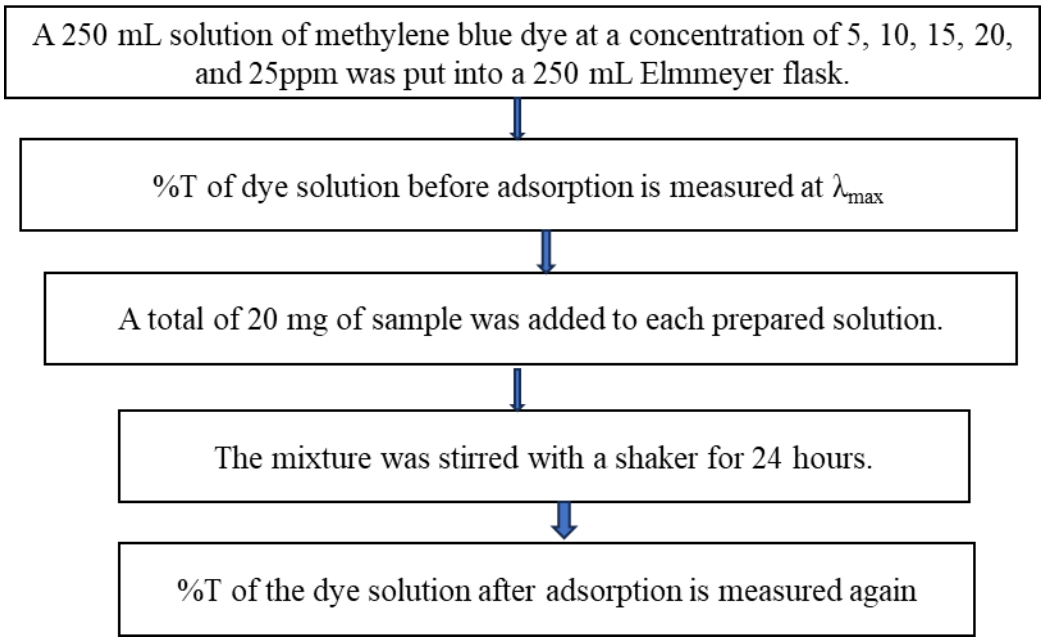

Scheme-2: How methylene blue adsorption works

The adsorption performance of the samples was tested using methylene blue at various concentrations. The samples tested were all samples, plus standard activated carbon as a comparison. The results of concentration measurements at the beginning and end of adsorption are used to determine the Langmuir adsorption isotherm. Adsorption isotherm analysis is used to determine the maximum adsorption capacity and adsorption isotherm constants. The adsorbent capacity at equilibrium is calculated from the adsorption process using Equation 1. The Langmuir adsorption isotherm equation is presented in Equation 2 [16].

$$q_e = (C_0 - C_e)\frac{V}{C\ adsorbent} \quad \text{(Eq. 1)}$$

$$\frac{C_e}{q_e} = \frac{1}{K_a.Q_m} + \frac{1}{Q_m} \times C_e \quad \text{(Eq. 2)}$$

Where q_e is the adsorption capacity at equilibrium, C_0 is the initial concentration, C_e is the equilibrium concentration. Adsorption data at various initial concentrations are plotted with a graph following equation 3.2 so that the maximum adsorption capacity (Q_m), and Langmuir constant (K_a) Can be determined [17]. Making cells for lithium battery anodes are shown in the following scheme 3.
How anode cell works analysed in scheme 3

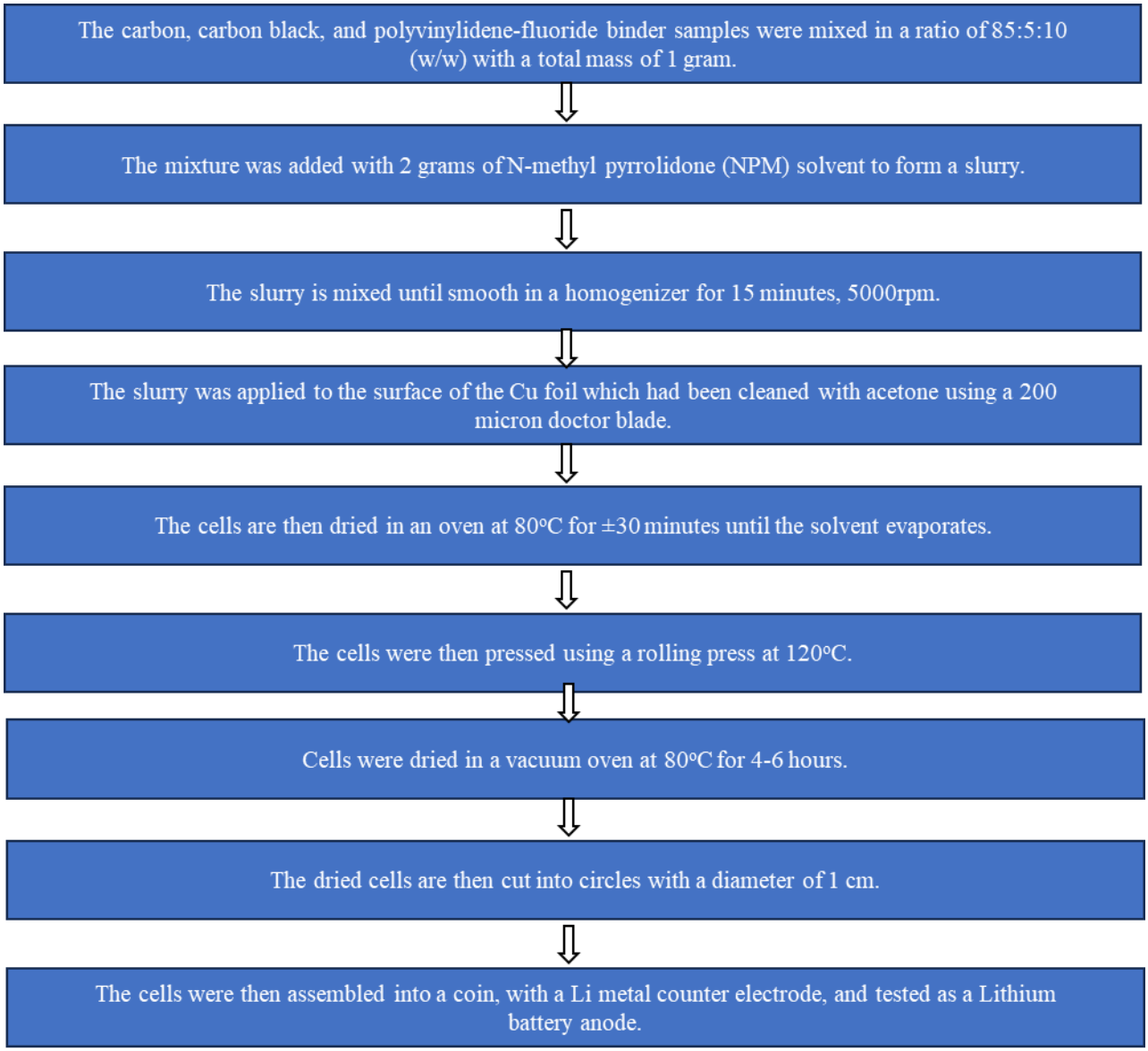

Scheme 3: How anode cell works

3. Results and Discussion

The effect of catalyst concentration on CNSs products was characterised by SEM-EDS, TEM, Raman, XRD, BET, and XPS analysis. In addition, initial application tests were carried out, namely the adsorption of methylene blue dye and CV tests as lithium battery anodes.

3.1. SEM Characterization

Visually, from the results of SEM analysis, it can be seen that the CNSs obtained are in the form of a conglomeration of spheres, not as a single sphere (Nieto-Marquez, Romero et al., 2010). In addition, as the catalyst concentration increases, the number of CNSs on the surface of AC increases. In addition, SEM tests were carried out for samples made without ferrocene catalysts, so it can be

believed that catalysts play a role in forming CNSs from cooking oil. The results of the SEM analysis are presented in Figure 1.

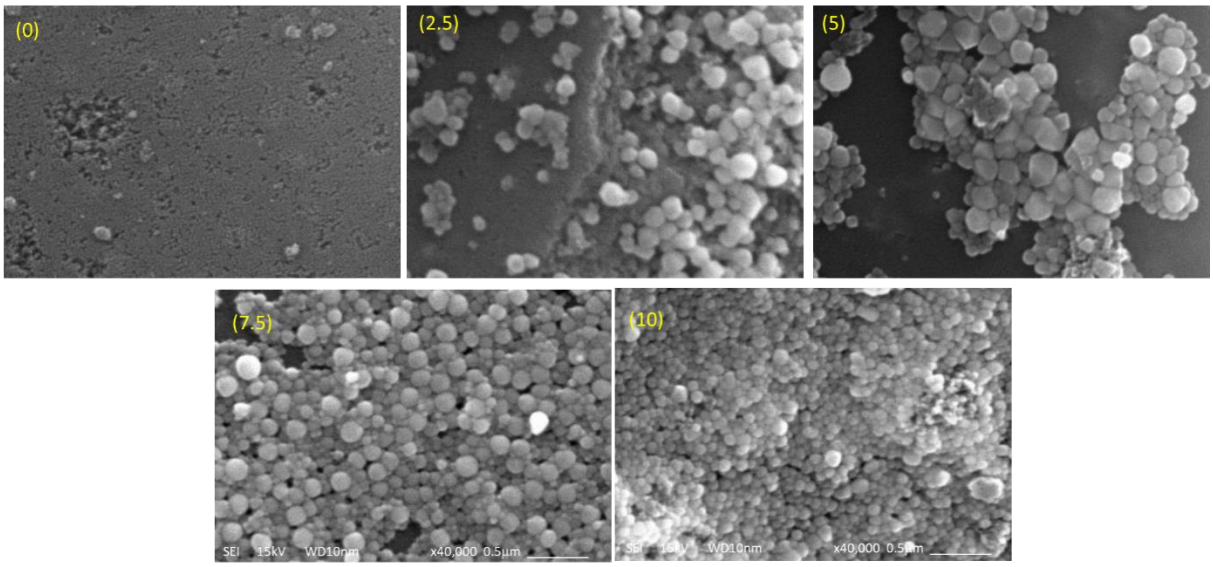

Figure 1: SEM analysis of CNSs with the catalyst at different concentrations of precursor

3.2 TEM Characterization

The presence of CNSs and iron catalysts can be observed more clearly in the TEM analysis presented in Figure 2. The results of the TEM analysis show that at small catalyst concentrations, the amount of CNSs produced is relatively small. Along with the increase in catalyst concentration, the amount of CNSs produced is also more significant, so it can be concluded that the catalyst concentration significantly affects the growth of CNSs. However, it can be observed from the TEM analysis that the particle size of CNSs produced on various catalyst variations is similar. This differs from the results obtained using the urea co-precipitation catalyst deposition method and ferrocene as the catalyst. In this study, along with the increase in catalyst, the number of CNSs observed from SEM and TEM analysis increased, was homogeneous, and was smaller [18-19]. This is thought to be caused by differences in catalyst deposition methods, where in this study, the ferrocene catalyst, which is well soluble in non-polar solvents, is mixed directly with the precursor so that its size depends on the solubility properties and ultimately does not provide a CNSs size that is much different in variations in catalyst concentration.

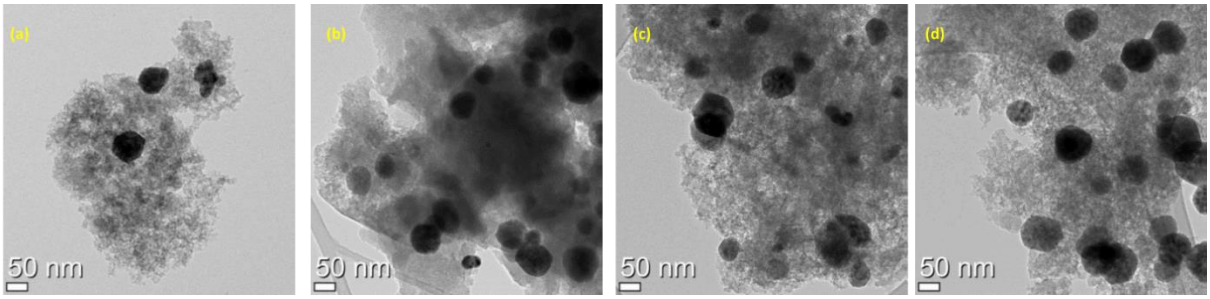

Figure 2: TEM analysis of CNSs with catalyst concentrations at (a) 2.5/100mL, (b) 5/100mL, (c) 7.5/100mL, and (d)10g/100mL. precursor

3.3. EDS Characterization

The presence of an iron catalyst can also be observed from the composition analysis results on the surface of AC using EDS (Table 1). It can be seen that along with the increase in the amount of catalyst used, there is an increase in the number of iron and oxygen atoms on the sample's surface. However, there is a deviation in the sample with a catalyst concentration of 10 g/100mL, where the concentration obtained is lower than that of 7.5 g/100mL. This deviation can be caused by the catalyst not being evenly distributed across the surface of the AC, so there is a deviation when the analysis is carried out. This is because the EDS analysis is local, only at one position being analysed, as in the example presented in Figure 3. Another exciting thing observed is the significant increase in the number of oxygen atoms, even more remarkable when compared to the supposed ratio between iron and oxygen in magnetite, which is 3:4. Some oxygen atoms are suspected to react with the carbon surface, either in activated carbon or nanocarbon, so that functional groups are formed on the surface of activated carbon.

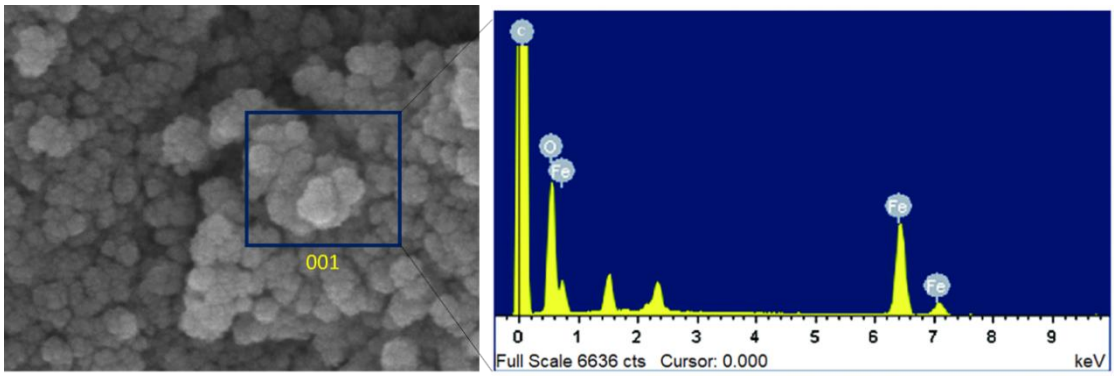

Figure 3: Example of EDS analysis results of CNSs with a catalyst concentration of 2.5g/100mL precursor

Table 1. EDS analysis results

Catalyst	% mass	% atomic

(g/100mL)	C	O	Fe	C	O	Fe
0	97.39	2.68	0.00	98.05	2.03	0.00
2.5	88.65	8.11	3.27	92.91	6.47	0.74
5	73.74	16.47	9.79	83.56	14.01	2.38
7.5	58.53	23.05	18.43	73.28	21.66	4.96
10	71.69	18.58	9.71	81.67	15.90	2.37

3.4. XRD Characterization

The results of XRD analysis at various catalyst concentrations are presented in Figure 4. From the results of the XRD analysis, it can be seen that all samples generally maintain the amorphous structure of activated carbon as a support for nanocarbon growth. In each sample, there are peaks at 27.1° and 42.8°, which indicate the sp^2 carbon C (0-0-2) and C (1-0-0) [20]. Meanwhile, Fe-peaks were observed at 29.7° (2-2-0), 36.1° (3-1-1), 45.4° (400), 58.5° (4-2-2), and 64.9° (4-4-0) [21], where the Miller Index is written in brackets. The XRD analysis showed the magnetite (Fe_3O_4) content on the surface of AC. When compared with the analysis of activated carbon without a catalyst as a control, presented in Figure 5, it can be seen that no sp2 carbon or iron peaks appear. The XRD curve of activated carbon without a catalyst shows broad peaks at 23˚-30˚ and 40˚, which indicate the amorphous carbon structure commonly found in activated carbon [22]. During pyrolysis the ferrocene catalyst undergoes decomposition based on the reaction: $Fe(C_5H_5)_2 \rightarrow Fe + C_xH_y$. The iron atoms released from ferrocene are the catalysts in synthesising nanocarbons. During the pyrolysis process, the oil used decomposes into simpler hydrocarbons, such as C_xH_y and $C_xH_yO_z$, in addition to the formation of CO and CO_2.[23] The carbon molecules from the oil decomposition will build the nanocarbon structure. It is suspected that the oxygen content from the oil decomposition then reacts with iron to form magnetite.

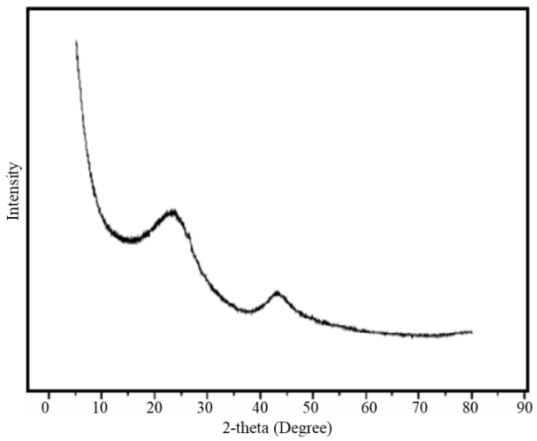

Figure 5. XRD analysis on samples without catalyst

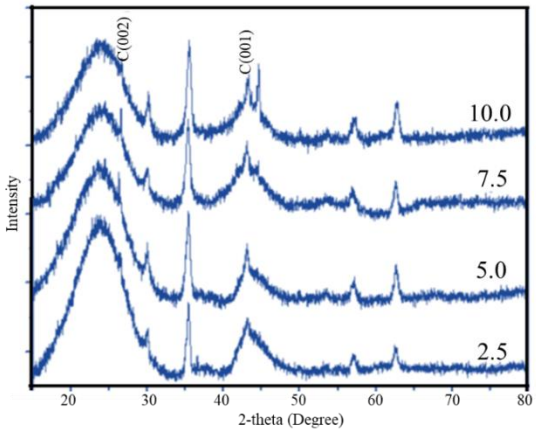

Figure 4: XRD analysis at various catalyst concentrations

3.5. BET Characterization

The characteristics of the pores of standard activated carbon and activated carbon deposited by CNSs are presented in Figure 6 and Table 2. Based on the adsorption isotherm curve, it can be concluded that the adsorption isotherm of the activated carbon sample shows type IV isotherm based on IUPAC, where the structure of the deposited activated carbon has a micropore-mesoporous structure. This is indicated by a hysteresis loop indicating nitrogen condensation in the mesopores of activated carbon [24].

The distribution of pores is presented in Figure 7. Based on the pore distribution, it can be seen that the products obtained are mostly micropores (<20Å) and mesopores (20-500Å), but the distribution of macropores is not observed. These results are consistent with those shown by the pore diameter measurement in Table 2. The iron catalyst and CNSs partially closed the pores, reducing the surface area and pore volume of activated carbon deposited by CNSs. However, increasing the amount of catalyst in the synthesis of CNSs did not provide significant changes to the surface area, pore volume or pore diameter. In the studies conducted by Nguyen et al. (2022) [25] prepared carbon nanofibers (CNFs) and Arie et al. (2016) prepared CNSs on the surface of AC, there was a decrease in the surface area and pore volume due to the closure of the pores by the nanocarbon product. The reduction in surface area in CNFs deposition reached 90%, and 96% in CNSs deposition. The nanocarbon products formed cover all the active carbon pores.

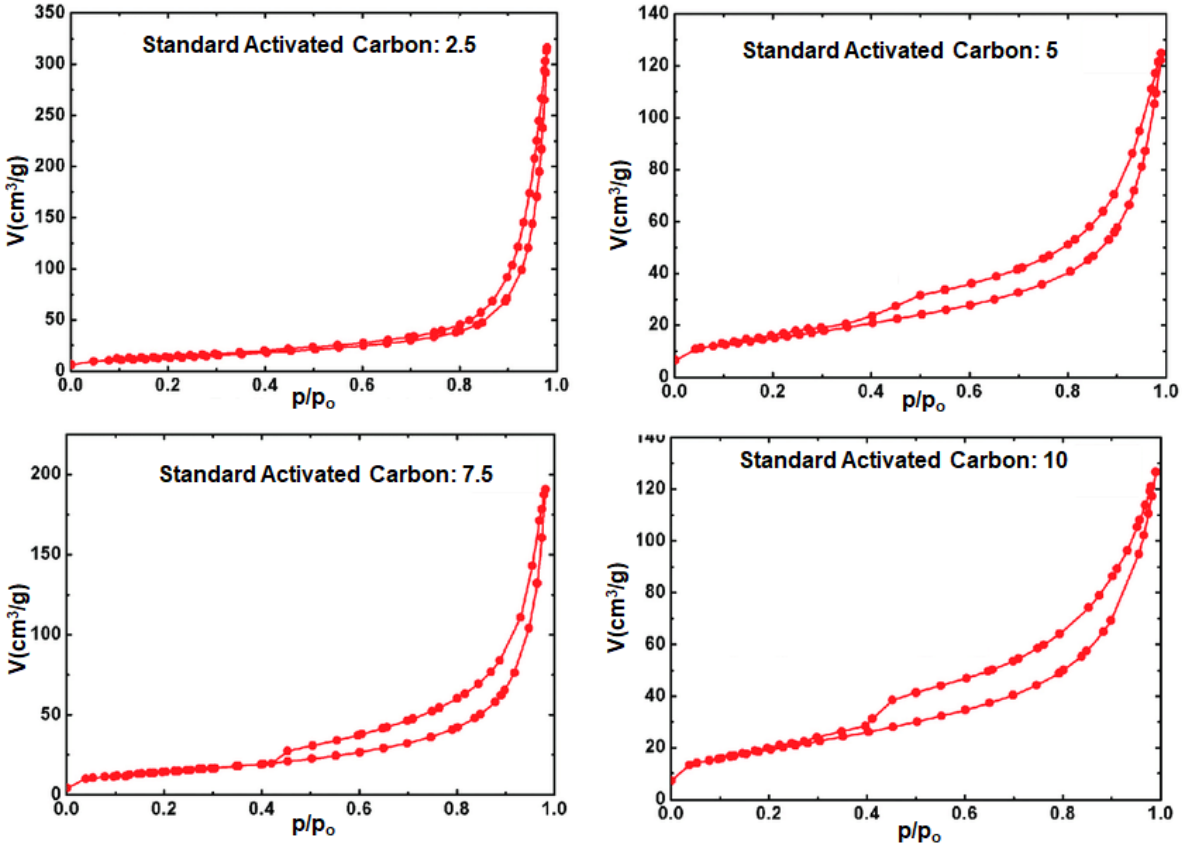

Figure 6. Adsorption isotherm curve

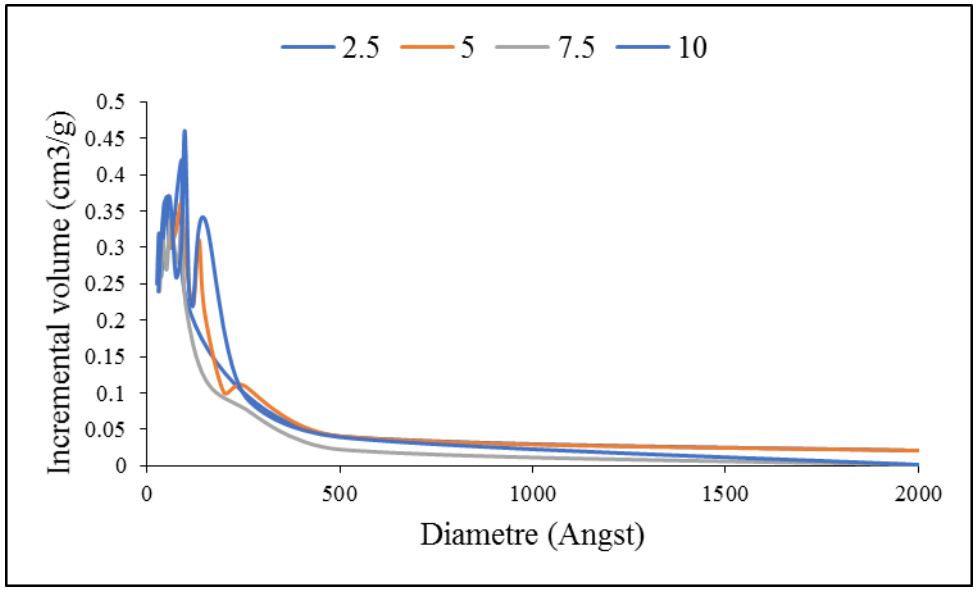

Figure 7. Distribution of BJH pores

Table 2. Sample pore characteristics

Sample	$BET\ surface\ area\ (m^2/g)$	$Pore\ Volume\ (cm^3/g)$	$Pore\ Diameter$ (Å)

AC Standard	781.05	0.64	33.27
2.5	492.15	0.46	37.47
5	488.59	0.47	38.88
7.5	464.91	0.45	39.08
10	488.76	0.47	39.02

3.6. Raman Characterization

Raman spectra of samples at various concentrations are presented in Figure 8. From the Raman spectra, it can be seen that all samples have peaks at 1334cm^{-1} (D-band) and 1597cm^{-1} (G-band). The D-band peak indicates a random graphite structure, while the G-band indicates a regular carbon structure [26]. A comparison of D-band (I_D) and G-band (I_G) intensities can be used to determine the characteristics of the obtained carbon products. A comparison of the I_D and IG of each sample is presented in Figure 9. The I_D/I_G value obtained is a typical value for the range of CNSs products, between 0.84 and 1.2 [27]. The difference in I_D/I_G values at catalyst concentrations of 2.5g/100mL can also be observed in 5, 7.5, and 10g/100mL catalysts. This shows that at low catalyst concentrations, the carbon nanostructures formed are still relatively few, so the carbon structure tends to be random (irregular). With the increase in catalyst, the carbon nanostructures formed become more, so that the G-band peak becomes more dominant, and it can be interpreted that the carbon product structure becomes

more graphitic. This is based on the results of the XRD spectra reading.

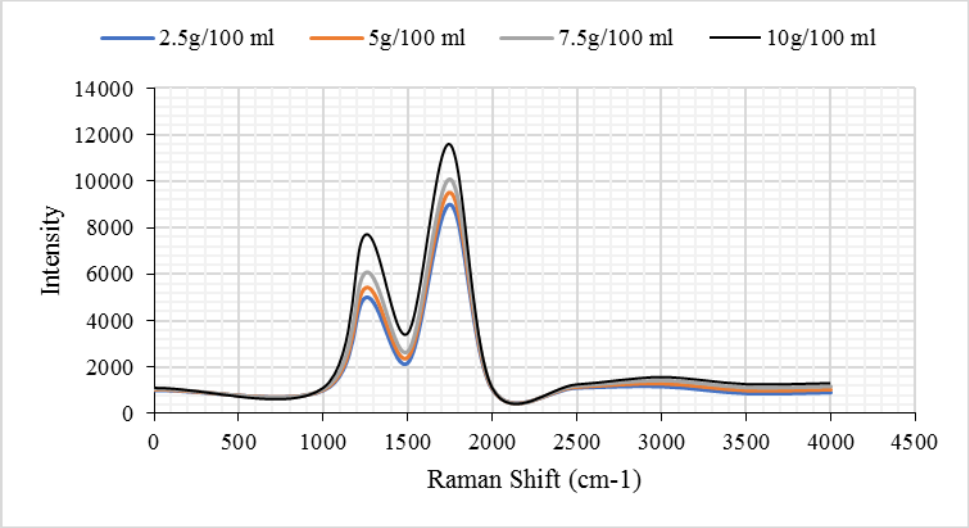

Figure 8. Raman spectra of samples at various concentrations

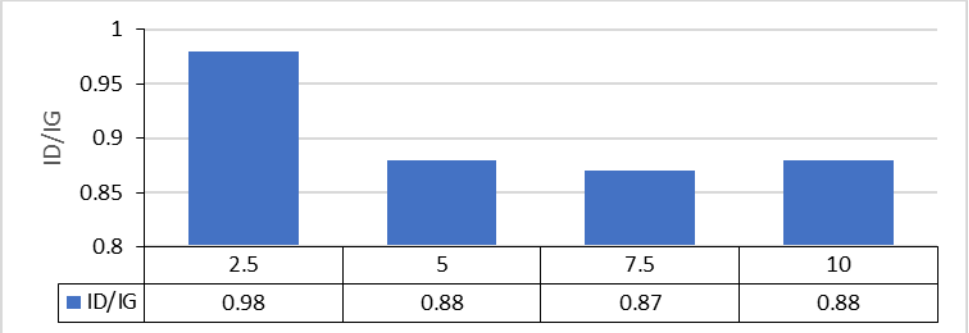

Figure 9. Comparison of I_D and I_G at various catalyst concentrations

3.7. XPS Characterization

An XPS analysis was carried out to confirm the suspicion of the formation of functional groups on the surface of activated carbon. An example of fitting on standard activated carbon for C1s is presented in Figure 10, and complete fitting data is presented in Table 3. All spectra observed a binding energy peak at around 284.5 eV, indicating a graphite structure, namely a C=C sp^2 double bond with no functional group [28]. All samples have a spectral peak at around 285.9-286.3 eV, indicating the presence of C-O- functional groups in phenol, alcohol, or ether bonds on the surface of activated carbon [29]. In addition, there is a peak at around 288.1-288.2 eV, indicating C atoms bonded to carboxyl or ester groups (-COO) on activated carbon [28-29].

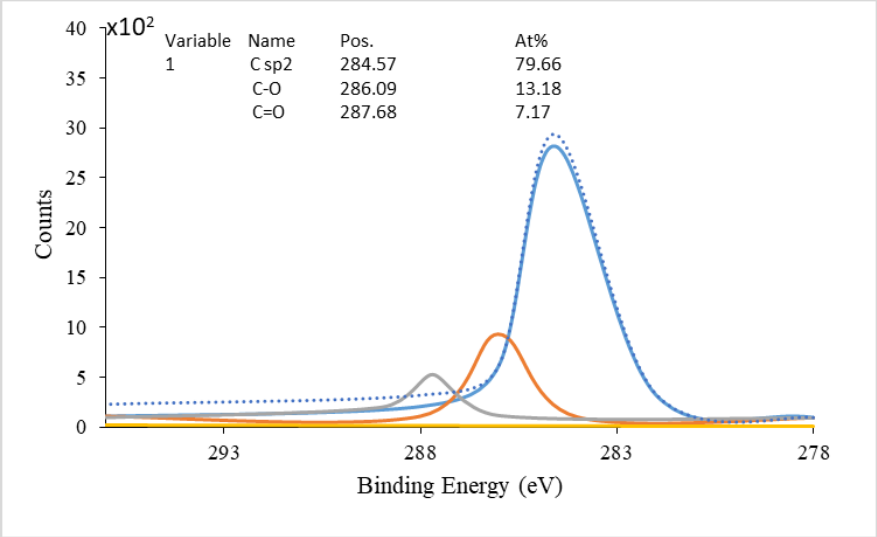

Figure 10. Fitting of C1s spectra for standard activated carbon samples

Table 3. Functional group composition of C1s spectra

	% Functional groups		
Catalyst (g/100mL)	C-sp^2	C-O	C=O
0	80.06	12.80	7.20
2.5	80.80	13.00	6.29
5	79.83	12.80	7.40
7.5	78.67	14.40	7.01
10	79.70	12.99	7.38

Based on the fitting results, it can be concluded that there is no significant difference in the amount of catalyst used for the functional groups on the sample surface. It is suspected that this can be caused by the amount of CNSs formed not too much or not covering the entire surface of the activated carbon so that the spectral analysis on the surface of the activated carbon still tends to maintain the composition of its functional groups.

3.8. Methylene blue adsorption test

The fitting results for the Langmuir adsorption isotherm are presented in Figure 11. The maximum adsorption capacity (Q_m) and the Langmuir adsorption constant parameters (K_a) are presented in Table 4. From the R^2 value, it can be seen that all samples give a value of almost 1, so it can be concluded that the

adsorption occurs in accordance with the Langmuir isotherm. Langmuir isotherm has an assumption that the adsorption that occurs is a reversible single-layer adsorption, with the rate-determining stage of adsorption being internal diffusion [30]. The Q_m value in all samples experienced a decrease of almost half in capacity. This is consistent with the decrease in the value of the AC surface area. It can be interpreted that the deposition of CNSs and magnetite content on the surface of activated carbon does not affect the adsorption of methylene blue. In a study by El-Bery et al. (2022) [31], the increased adsorption capacity of activated carbon was due to increased functional groups that increased the adsorption capacity. Different results were obtained in this study due to no changes in the functional groups of activated carbon, as presented in Table 4, so the effect of the surface area of activated carbon on the adsorption capacity became more dominant.

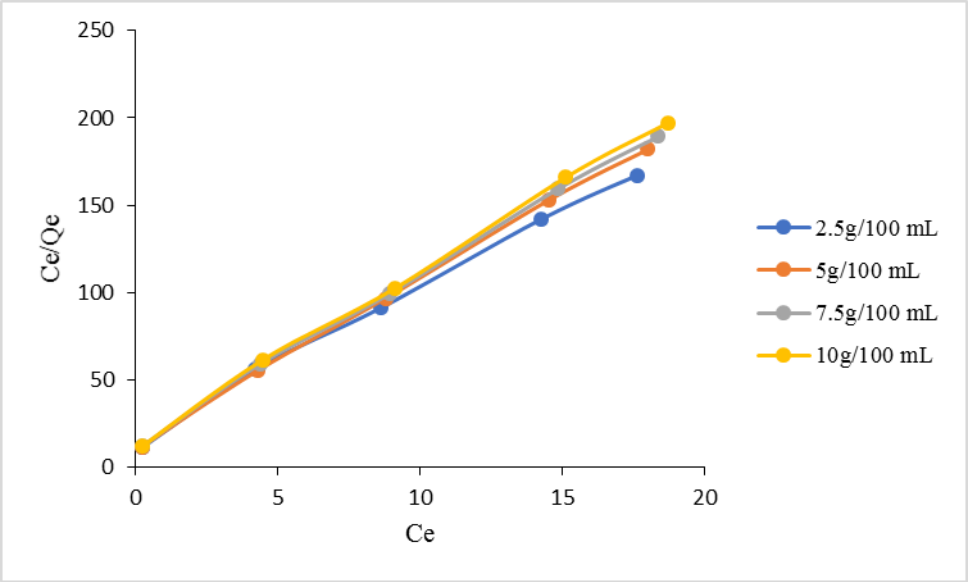

Figure 11: $\frac{Ce}{qe} vs. Ce$ curve for various samples

Table 4. Adsorption capacity and Kinetic parameters for the MB removal

	Catalyst (g/100mL)				
Parameter	0	2.5	5	7.5	10
Q_m	0.2188	0.0862	0.0910	0.0932	0.0957
K_a	0.8240	0.7922	0.4747	1.0422	0.8687
R^2	1.0126	1.0171	1.0137	1.0156	1.0109

3.9. Performance test as lithium battery anode with CV

The electrochemical performance of the sample with a catalyst concentration of 2.5g/100mL was tested using cyclic voltammetry (CV). The CV voltammogram curve is presented in Figure 12. In the first cycle, a peak can be seen in the reduction area around 0.25-1.0V, indicating the formation of a solid electrolyte interphase (SEI) [32]. This peak was no longer visible in the second and third cycles. Meanwhile, in each cycle, an oxidation peak was observed at around 0.3V, indicating the existence of an intercalation/deintercalation mechanism of lithium ions in the charge-discharge process [32]. The magnetite content in the sample did not affect the cycle, as indicated by the absence of peaks other than lithium intercalation appearing in the voltammogram. If the iron content in the sample played a role in the cycle, a cathode peak would appear at 0.9V and a reduction peak at 1.65V [33,34]. From the voltammogram obtained, it can be concluded that the CNSs sample on activated carbon with a catalyst of 2.5g/100mL is stable when used as an anode for lithium batteries. Further tests such as Galvanostatic Charge-Discharge, rate cycle, and impedance can be carried out to determine the CNSs sample's performance further.

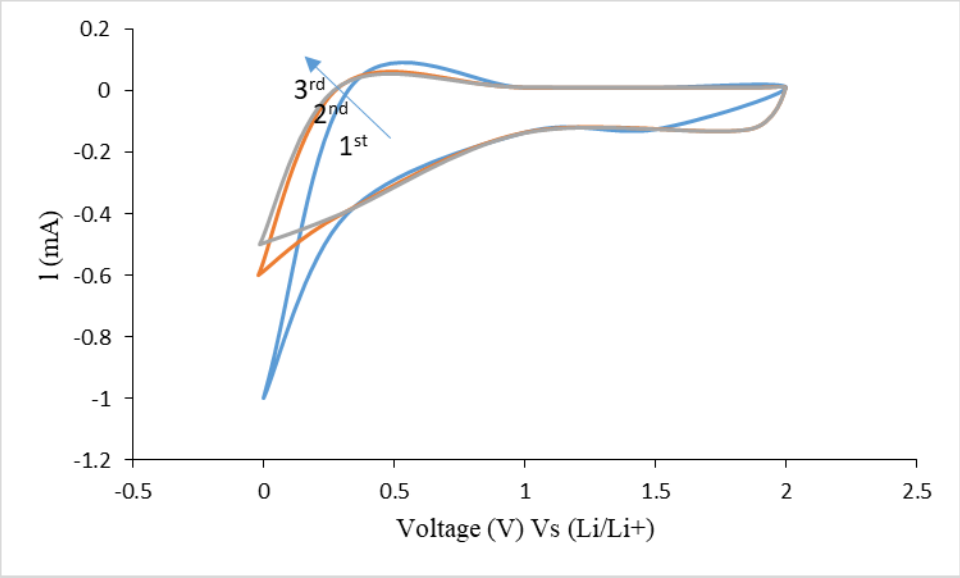

Figure 12: Voltammogram for the sample with 2.5g/100mL catalyst

Conclusion:

Based on the research, it can be concluded that the greater the amount of catalyst used, the more CNSs are deposited on the AC surface, which aligns with the results shown by SEM, TEM, XRD, and Raman analysis. The amount of catalyst added does not affect the functional groups on the AC surface. When

used as an adsorbent, the sample's performance decreases, along with a reduction in surface area due to the deposition of CNSs and catalysts on the AC surface. The performance of the sample with a catalyst of 2.5g/100mL provides stable performance when used as a lithium battery anode, as shown by the half-cell CV test with a voltage range of 0-2V and a scan rate of 0.2mV/s.

Based on the research conducted, there are several suggestions as follows:

1. The homogeneity of the mixture of ferrocene catalyst, cooking oil, and activated carbon can be improved by mixing and impregnation before carbonisation

2. Several studies that need to be carried out, such as the effect of washing to remove iron catalysts and application tests as adsorbents and lithium battery anodes, can be studied further.

References

[1]. GERGEROGLU, Hazal; YILDIRIM, Serdar; EBEOGLUGIL, Mehmet Faruk. Nano-carbons in biosensor applications: An overview of carbon nanotubes (CNTs) and fullerenes (C60). *SN Applied Sciences*, 2020, 2.4: 603.

[2]. GUTIÉRREZ-GARCÍA, Carmen Judith, et al. Synthesis of carbon spheres by atmospheric pressure chemical vapor deposition from a serial of aromatic hydrocarbon precursors. *Physica E: Low-dimensional Systems and Nanostructures*, 2019, 112: 78-85.

[3]. SHI, Liang, et al. Controlled growth of carbon spheres through the Mg-reduction route. *Nanoscale research letters*, 2010, 5: 20-24.

[4]. ISAEVA, Vera I., et al. Modern carbon–based materials for adsorptive removal of organic and inorganic pollutants from water and wastewater. *Molecules*, 2021, 26.21: 6628.

[5]. HEIDARI, Ava; YOUNESI, Habibollah. Synthesis, characterization and life cycle assessment of carbon nanospheres from waste tires pyrolysis over ferrocene catalyst. *Journal of Environmental Chemical Engineering*, 2020, 8.2: 103669.

[6]. ALGADRI, Natheer A., et al. Effect of ferrocene catalyst particle size on structural and morphological characteristics of carbon nanotubes grown by microwave oven. *Journal of Materials Science*, 2017, 52: 12772-12782.

[7]. WULAN, Praswasti PDK; RIVAI, Ghassan Tsabit. Synthesis of carbon nanotube using ferrocene as carbon source and catalyst in a vertical structured catalyst reactor. In: *E3S Web of Conferences*. EDP Sciences, 2018. p. 03038.

[8]. KRISTIANTO, Hans, et al. Synthesis and characterization of carbon nanospheres using cooking palm oil as natural precursors onto activated carbon support. *Procedia chemistry*, 2015, 16: 328-333.

[9]. JIN, Yi Zheng, et al. Large-scale synthesis and characterization of carbon spheres prepared by direct pyrolysis of hydrocarbons. *Carbon*, 2005, 43.9: 1944-1953.

[10]. ZHANG, Junhao, et al. Synthesis, characterization and properties of carbon nanotubes microspheres from pyrolysis of polypropylene and maleated polypropylene. *Materials Research Bulletin*, 2010, 45.1: 15-20.

[11]. LOU, Zirui, et al. Carbon sphere template derived hollow nanostructure for photocatalysis and gas sensing. *Nanomaterials*, 2020, 10.2: 378.

[12]. NÁFRÁDI, Bálint, et al. Room temperature manipulation of long lifetime spins in metallic-like carbon nanospheres. *Nature communications*, 2016, 7.1: 12232.
[13]. ARIE, Arenst Andreas, et al. Effect of Catalyst Preparation Method on the Characteristics of Carbon Nanospheres as Anode Materials of Lithium Secondary Batteries. *Advanced Materials Research*, 2015, 1123: 308-311.
[14]. KRISTIANTO, Hans, et al. The effect of activated carbon support surface modification on characteristics of carbon nanospheres prepared by deposition precipitation of Fe-catalyst. In: *IOP Conference Series: Materials Science and Engineering*. IOP Publishing, 2016. p. 012034.
[15]. KARNA, Priya, et al. Synthesis and characterization of carbon nanospheres. *Open Access Library Journal*, 2017, 4.05: 1.
[16]. KHAMSEH, Ali A. Gh, et al. Investigation of kinetic, isotherm and adsorption efficacy of thorium by orange peel immobilized on calcium alginate. *Scientific Reports*, 2023, 13.1: 8393.
[17]. MUSTAPHA, S., et al. Adsorption isotherm, kinetic and thermodynamic studies for the removal of Pb (II), Cd (II), Zn (II) and Cu (II) ions from aqueous solutions using Albizia lebbeck pods. *Applied water science*, 2019, 9: 1-11.
[18]. NIETO-MÁRQUEZ, Antonio, et al. Carbon nanospheres: synthesis, physicochemical properties and applications. *Journal of Materials chemistry*, 2011, 21.6: 1664-1672.
[19]. GUPTA, Aayush; KOUR, Rajpal; BRAR, Loveleen K. Facile synthesis of carbon nanospheres from saccharides for photocatalytic applications. *SN Applied Sciences*, 2019, 1: 1-8.
[20]. ARIE, Arenst Andreas, et al. Structural and preliminary electrochemical characteristics of palm oil based carbon nanospheres as anode materials in lithium ion batteries. *Carbon letters*, 2016, 18: 80-83.
[21]. KOBYLIUKH, Anastasiia, et al. Effect of graphene material structure and iron oxides deposition method on morphology and properties of graphene/iron oxide hybrids. *Applied Surface Science*, 2022, 573: 151567.
[22]. SHAHCHERAGH, S. K.; BAGHERI MOHAGHEGHI, M. M.; SHIRPAY, A. Effect of physical and chemical activation methods on the structure, optical absorbance, band gap and urbach energy of porous activated carbon. *SN Applied Sciences*, 2023, 5.12: 313.
[23]. BANCHAPATTANASAKDA, Warintorn; ASAVATESANUPAP, Channarong; SANTIKUNAPORN, Malee. Conversion of waste cooking oil into bio-fuel via pyrolysis using activated carbon as a catalyst. *Molecules*, 2023, 28.8: 3590.
[24]. THOMMES, Matthias, et al. Physisorption of gases, with special reference to the evaluation of surface area and pore size distribution (IUPAC Technical Report). *Pure and applied chemistry*, 2015, 87.9-10: 1051-1069.
[25]. NGUYEN, Trong Danh; LEE, Jun Seop. Electrospinning-based carbon nanofibers for energy and sensor applications. *Applied Sciences*, 2022, 12.12: 6048.
[26]. Roslan, M. S., Chaudary, K. T., Haider, Z., Zin, A. F. M., & Ali, J. Effect of magnetic field on carbon nanotubes and graphene structure synthesized at low pressure via arc discharge process. In *AIP Conference Proceedings* .(2017, March). (Vol. 1824, No. 1). AIP Publishing.
[27]. HU, Kaiyue, et al. Development of tailored graphene nanoparticles: Preparation, sorting and structure assessment by complementary techniques. *Molecules*, 2023, 28.2: 565.
[28]. ALIYEV, Elvin, et al. Structural characterization of graphene oxide: Surface functional groups and fractionated oxidative debris. *Nanomaterials*, 2019, 9.8: 1180.
[29]. SAYĞILI, H.; GÜZEL, F. Usability of activated carbon with well-developed mesoporous structure for the decontamination of malachite green from aquatic environments: kinetic, equilibrium and regeneration studies. *Journal of Porous Materials*, 2018, 25: 477-488.

[30]. LÓPEZ-LUNA, Jaime, et al. Linear and nonlinear kinetic and isotherm adsorption models for arsenic removal by manganese ferrite nanoparticles. *SN Applied Sciences*, 2019, 1: 1-19.
[31]. EL-BERY, Haitham M., et al. High adsorption capacity of phenol and methylene blue using activated carbon derived from lignocellulosic agriculture wastes. *Scientific reports*, 2022, 12.1: 5499.
[32]. ZHANG, Yi, et al. Porous amorphous silicon hollow nanoboxes coated with reduced graphene oxide as stable anodes for sodium-ion batteries. *ACS omega*, 2022, 7.34: 30208-30214.
[33]. SHENG, Lin, et al. Advances and challenges in electrolyte development for magnesium–sulfur batteries: a comprehensive review. *Molecules*, 2024, 29.6: 1234
[34]. ABAAS, H. J.; AL-JEBOORI, M. J. New dimeric complexes with semicarbazone mannish-based ligand; formation, structural investigation and biological activity. Revis Bionatura 2023; 8 (2) 15. In: *Journal of Physics: Conference Series*. s Note: Bionatura stays neutral with regard to jurisdictional claims in published maps and institutional affiliations., 2021. p. 3-20.